Z. Angew. Math. Phys. (2016) 67:95

0044-2275/16/040001-17
published online July 22, 2016
DOI 10.1007/s00033-016-0692-5

Zeitschrift für angewandte Mathematik und Physik ZAMP

Numerical identification procedure between a micro-Cauchy model and a macro-second gradient model for planar pantographic structures

Ivan Giorgio

Abstract. In order to design the microstructure of metamaterials showing high toughness in extension (property to be shared with muscles), it has been recently proposed (Dell'Isola et al. in Z Angew Math Phys 66(6):3473–3498, 2015) to consider pantographic structures. It is possible to model such structures at a suitably small length scale (resolving in detail the interconnecting pivots/cylinders) using a standard Cauchy first gradient theory. However, the computational costs for such modelling choice are not allowing for the study of more complex mechanical systems including for instance many pantographic substructures. The microscopic model considered here is a quadratic isotropic Saint-Venant first gradient continuum including geometric nonlinearities and characterized by two Lamé parameters. The introduced macroscopic two-dimensional model for pantographic sheets is characterized by a deformation energy quadratic both in the first and second gradient of placement. However, as underlined in Dell'Isola et al. (Proc R Soc Lond A 472(2185):20150790, 2016), it is needed that the second gradient stiffness depends on the first gradient of placement if large deformations and large displacements configurations must be described. The numerical identification procedure presented in this paper consists in fitting the macro-constitutive parameters using several numerical simulations performed with the micro-model. The parameters obtained by the best fit identification in few deformation problems fit very well also in many others, showing that the reduced proposed model is suitable to get an effective model at relevantly lower computational effort. The presented numerical evidences suggest that a rigorous mathematical homogenization result most likely holds.

Mathematics Subject Classification. 74A30 · 74B20 · 74S05.

Keywords. Nonlinear elasticity · Second gradient models · Elastic surface theory · Numerical parameter identification.

1. Introduction

In recent years, the new concept of conceiving tailored materials has been developed: These artificial materials are architectured to produce exotic or adaptive behavior and are some times called metamaterials [28]. These last are characterized by 'ad hoc' microstructure whose mechanical properties could be induced by an internal architecture which is designed in order to exhibit an unexpected behavior useful in some specific applications. In Ref. [2,92], for instance, are introduced truss microstructures that in the homogenized limit produces two-dimensional elastic materials with uncommon mechanical interactions which cannot be described at a macro-scale in the classical framework of Cauchy stress theory. Following this way of thinking, we study a mechanical system (see Fig. 1) that can be called pantographic structure (see [34,40,53,102]) because can be regarded as a net of 'fibers' arranged in such a way that a small deformation of each fiber could results in a large deformation of the whole sample. In Ref. [34], experimental bias extension tests shows three specific areas under the stress–strain curve. Addition to the usual linear elastic regime, a nonlinear elastic behavior zone can be distinguished, and thereafter, a zone, in which begin to occur the first breaks, characterized by a further significant increase of the resultant force which the material is capable of sustaining. As a result, this structure is characterized by a high toughness, i.e., a sample is able to absorb a large amount of energy, beyond the elastic regime, plastically deforming before failure. Furthermore, because the energy is concentrated in certain well-defined locations, i.e., the

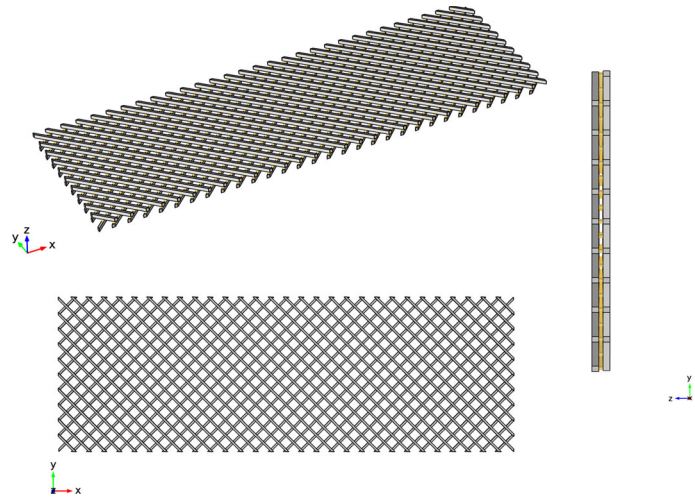

FIG. 1. Sample topology

four corners and the connecting pivots in the central area, the failure mechanism can easily predict on the basis of the type of deformation and of the material of which the specimen is made. For instance, in a bias extension test, more the material is brittle, the more the failure is expected into central areas; on the contrary, more the material is ductile, the more the failure will occur in the four corners and progressively on the clamped edges. Finally, this material shows also an advantageous strength-to-weight ratio, making it particularly attractive in many applications both in the industrial and aerospace world.

The description of these pantographic structures could be fully addressed by means of classical continuum theories, as for instance, a Cauchy-type continuum model; however, although it is possible to describe in detail the mechanical behavior of the system, considering such a model entails great computational efforts. Alternatively, a generalized continuum theory could be employed in which more kinematical descriptors are introduced to capture the features induced by the microstructure at a scale sufficiently large to neglect the geometrical details of the same microstructure. The viewpoint taken in the present paper is to adopt a Cauchy continuum model as a reference one and compare it with a generalized model in order to validate and to assess the range of applicability of this latter with a suitable parameter estimation. As a result, the generalized model could be considered as a more nimble and flexible tool for calculating and forecasting. This point of view is not new, in fact, the need to include in continuum theories the description of long range interaction between the material particles, it has already been dealt with in the pioneer works of Piola [36] who considered the possibility to postulate a deformation energy of continua including second and possibly higher gradients of placement.

In this framework of generalized continuum, accounting for different microstructural features, many elastic theories have been introduced as micromorphic [44,52], micropolar [3,4,6,42,43,51,61], higher gradient [35,37,38,72,73,98] and non-local continua [30,45]. In particular, to address the problem of characterizing net of fibers, we can refer to models which in different ways take into account the deformation of the fibers; indeed, some models are formulated assuming the fibers to be inextensible [22,31,32,34,39,96], others including the resistance to stretch, shear distortion [39,94–96], bending [23,39,89,90] and also twist [94,95]. These kind of models can be obtained with proper homogenization procedures starting from suitable microstructures (see, e.g., [1,13,33,42,54,64,77]) and can be employed to describe the mechanical behavior of a large set of material both artificial materials as membrane structures [10,56,60,71], fiber-reinforced composites or synthetic textile materials [9,65–68,75,76,91], and fiber-reinforced biological tissues as articular cartilage with collagen fibers [47,48,62,63,97] or trabecular bone [55,69].

At this point, some considerations are needed concerning the macro-models which can be introduced for pantographic structures. These models based on higher gradient continua involve more material parameters than the classical Cauchy medium, therefore 'ad hoc' tools are required to evaluate them (see, e.g., [14,27,41,49,70,81,82,93,99]). Moreover, second gradient elasticity needs a formulation developed to properly approximate solutions in the Sobolev space H^2, and hence, a standard finite element analysis is not optimized in this context. On the other hand, newly developed numerical tools can be profitably employed to avoid this lack of formulation (see, e.g., [15–19,29,57–59,100,101]).

In conclusion, some challenges and future perspectives are worth noting for these macro-models based on generalized continua as issues related to dissipation which can be caused by different sources [11,12,74] damage evolution and detection [24,79,80,83,87,103,104], as well as contacts and soft impacts [7,8] and unusual behavior such as strain localization related to buckling under certain critical loads [5,20,21,25,26,46,50,78,84–86,88].

Summarizing, in this paper, we perform a micro–macro identification for planar pantographic structures. In Sect. 2, we recall the basic kinematics of the two models employed for the identification procedure, following a standard Cauchy continuum theory for the micro-model and [33] for the macro-second gradient model. The results of the parameter estimation are outlined and discussed in Sect. 3.

2. Pantographic structure modeling

Herein, a Cauchy continuum model which describes in details the considered pantographic structure is used as reference model to test and validate the more efficient—from a computational point of view—macro-model adopted here following the reasons exposed in [33]. In what follows, a concise description of the two models adopted is provided.

2.1. Micro-model

In the framework of a Lagrangian description of Kinematics, let $\boldsymbol{X} \in \mathscr{B} \subset \mathbb{R}^3$ be the position of a material particle in the reference configuration and let its image $\boldsymbol{x}$ through the map $\boldsymbol{\chi}: \mathscr{B} \to \mathbb{R}^3$ be its position in the current configuration. Accordingly, with classical notation, we introduce the deformation gradient tensor $\boldsymbol{F} = \nabla\boldsymbol{\chi}$ and subsequently the Green–St-Venant strain tensor as follows

$$\boldsymbol{E} = \frac{1}{2}\left(\boldsymbol{F}^{\mathrm{T}}\boldsymbol{F} - \boldsymbol{I}\right). \tag{2.1}$$

By introducing the displacement

$$\boldsymbol{u}(\boldsymbol{X}) = \boldsymbol{\chi}(\boldsymbol{X}) - \boldsymbol{X} \tag{2.2}$$

we can recast Eq. (2.1) as

$$\boldsymbol{E}(\boldsymbol{X}) = \frac{1}{2}\left(\nabla\boldsymbol{u} + \nabla\boldsymbol{u}^{\mathrm{T}} + \nabla\boldsymbol{u}^{\mathrm{T}}\nabla\boldsymbol{u}\right) \tag{2.3}$$

highlighting the geometric nonlinearity in terms of $\nabla\boldsymbol{u}$. Assuming the constitutive relation for isotropic and homogeneous materials, the Piola stress tensor can be evaluated as

$$\boldsymbol{T} = \lambda\,\mathrm{tr}\boldsymbol{E}\,\boldsymbol{I} + 2\mu\,\boldsymbol{E} \tag{2.4}$$

where λ and μ are the Lamé parameters. Furthermore, the strain energy density is defined as

$$W_m(\boldsymbol{E}) = \frac{1}{2}\boldsymbol{T} : \boldsymbol{E}. \tag{2.5}$$

The governing equations are derived from Eq. (2.5) by means of a variational principle as follows

$$\delta \int_{\mathscr{B}} W_m(\boldsymbol{E})\, \mathrm{d}\mathscr{B} = 0 \quad \forall\ \delta \boldsymbol{u}. \tag{2.6}$$

2.2. Macro-model

To describe the samples under study at macro-level, we consider the model presented in [33]. Therein, a micro-structured two-dimensional continuum made up of two families of orthogonal fibers, arranged as the beams in Fig. 1, is employed. This model, suitable for plane motion, accounts for stretching, bending and shear resistance related to the angle change between fibers belonging to different families.

By introducing a Lagrangian basis $\mathbf{D}_\alpha,\ \alpha = \{1, 2\}$ oriented along the two families of fibers, the current position $\boldsymbol{x}$ of a material point can be made explicit as

$$\boldsymbol{x} = \boldsymbol{\chi}(\boldsymbol{X}) = (X^\alpha + u^\alpha(X^\beta))\mathbf{D}_\alpha \tag{2.7}$$

i.e., as function of the position $\boldsymbol{X}$ in the reference configuration through the map $\boldsymbol{\chi} : \Omega \to \mathbb{R}^2$, being Ω a rectangular plane region. Of course, the particular expression of the map $\boldsymbol{\chi}$ in Eq. (2.7) is dictated by the fiber Kinematics. Also in this context, we set $\boldsymbol{F} = \nabla\boldsymbol{\chi}$. The field of unit vectors tangent to the fibers in the current configuration can be obtained by

$$\boldsymbol{e}_\alpha = \frac{\boldsymbol{F}\mathbf{D}_\alpha}{\|\boldsymbol{F}\mathbf{D}_\alpha\|}. \tag{2.8}$$

Moreover, the auxiliary vector field $\boldsymbol{c}_\alpha$ is introduced as

$$\boldsymbol{c}_\alpha = \frac{\nabla\boldsymbol{F}\ |\boldsymbol{D}_\alpha \otimes \boldsymbol{D}_\alpha}{\|\boldsymbol{F}\mathbf{D}_\alpha\|} \tag{2.9}$$

where $(\nabla\boldsymbol{F}\ |\mathbf{D}_\alpha \otimes \mathbf{D}_\alpha)^\beta = \partial_\alpha F^\beta_\alpha = \partial_{\alpha\alpha}\chi^\beta$.

For this kind of micro-structured two-dimensional continuum, we introduce as tailored strain measures the *stretch of fibers*

$$\varepsilon_\alpha = \|\boldsymbol{F}\mathbf{D}_\alpha\| - 1, \tag{2.10}$$

the *fiber curvature*

$$\kappa_\alpha = \|\boldsymbol{c}_\alpha - (\boldsymbol{c}_\alpha \cdot \boldsymbol{e}_\alpha)\, \boldsymbol{e}_\alpha\| = \|(\boldsymbol{I} - \boldsymbol{e}_\alpha \otimes \boldsymbol{e}_\alpha)\, \boldsymbol{c}_\alpha\|\,, \tag{2.11}$$

which considers each fiber as a beam axially deformable and shear undeformable and takes bending deformation of the fibers into account, the *shear distortion* γ, i.e., the change in the angle between the fibers defined by

$$\sin(\gamma) = \boldsymbol{e}_1 \cdot \boldsymbol{e}_2. \tag{2.12}$$

A strain energy density incorporating all these contributions is assumed to be

$$W_M(\varepsilon_\alpha, \kappa_\alpha, \gamma) = \sum_\alpha \left(\frac{1}{2}K_I\varepsilon_\alpha^2 + \frac{1}{2}K_{II}\kappa_\alpha^2\right) + \frac{1}{2}K_p\gamma^2 \tag{2.13}$$

where the material parameters K_I, K_{II} and K_p are positive and constant.

As done for the micro-model, also in this case, we use a variational principle to obtain the governing equations:

$$\delta \int_\Omega W_M(\varepsilon_\alpha, \kappa_\alpha, \gamma)\, \mathrm{d}\Omega = 0 \quad \forall\ \delta \boldsymbol{u}. \tag{2.14}$$

TABLE 1. *Characteristic dimensions of pantographic samples*

Sample n.	a (mm)	b (mm)	h_p (mm)	d_p (mm)	h_p/d_p	p (mm)
1	0.9	1.6	1	0.9	1.11	4.85
2	0.9	1.6	0.5	0.9	0.56	4.85
3	0.9	1.6	1	1.2	0.83	4.85
4	0.9	1.6	0.5	1.2	0.42	4.85
5	0.9	1.6	1	1.6	0.62	4.85
6	0.9	1.6	0.5	1.6	0.31	4.85

TABLE 2. *Mechanical properties of Polyamide PA 2200*

Mechanical properties	Values
Mass density	930 kg/m^3
Young modulus	1600 MPa
Poisson ratio	0.3

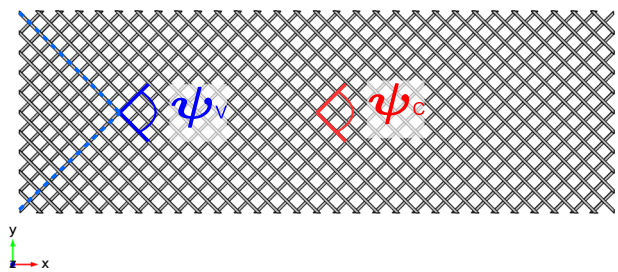

FIG. 2. Two control angles employed in the identification procedure

TABLE 3. *Identified stiffnesses of pantographic sheets*

Sample	K_{I} (N m^{-1})	K_{II} (N m)	K_p (N m^{-1})
1	6.164×10^5	1.299×10^{-2}	1.076×10^3
2	6.537×10^5	1.443×10^{-2}	1.600×10^3
3	5.929×10^5	1.443×10^{-2}	2.582×10^3
4	6.385×10^5	1.443×10^{-2}	3.556×10^3
5	6.461×10^5	2.886×10^{-2}	6.197×10^3
6	7.601×10^5	3.607×10^{-2}	7.229×10^3

3. Numerical macro-parameter identification

In the present section, comparing the two aforementioned models, an identification of the material parameters of the homogenized continuum macro-model is carried out via a best fit, employing suitable cost functions. In detail, we perform bias extension test simulations using the two models under the same conditions for six different kinds of samples and compare the overall stored energy and some representative deformations at points chosen specifically for this purpose.

The shape of the sample is a rectangle of size 0.06987×0.2096 m. The microstructure is constituted by 'beams', whose geometry is a rectangular cross section of size $a \times b$, the same for all the samples and different connector-pivots with height h_p and diameter d_p, as listed in Table 1. The material adopted for the numerical simulations performed with the micro-model is the polyamide PA 2200, whose material properties are shown in Table 2.

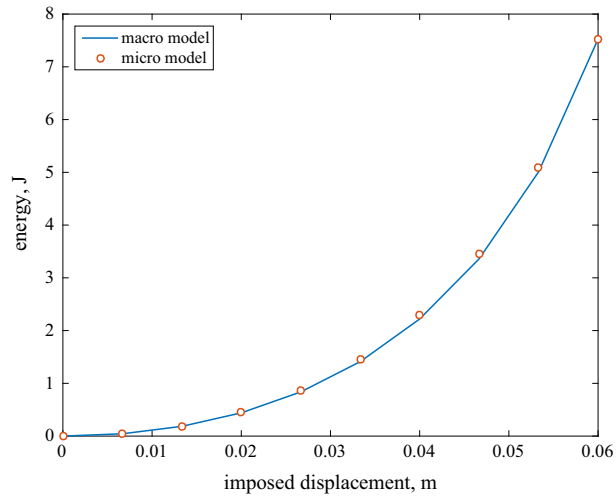

FIG. 3. Sample n. 1: Comparison of the total energy between the micro-Cauchy model (*points*) and the macro-second gradient model (*solid line*)

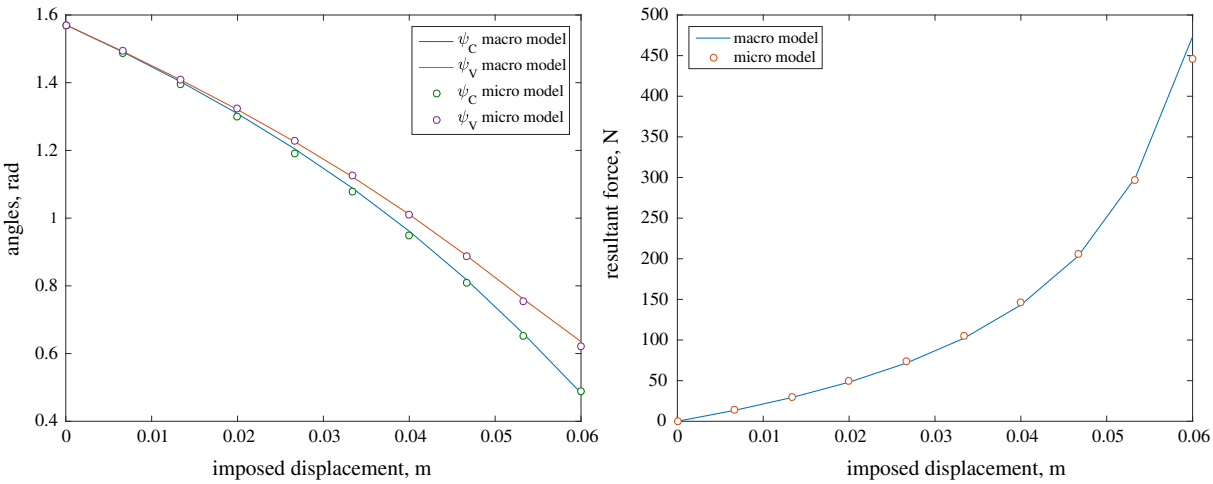

FIG. 4. Sample n. 1: Comparisons between the micro-Cauchy model (*points*) and the regression with a macro-second gradient model (*solid line*). Angle at the center ψ_C (*blue line*), angle at the corner ψ_V (*red line*) on the *left*; total reaction on the *right* (color figure online)

In the identification procedure, we estimate the material parameters of the macro-model K_{I}, K_{II} and K_p using deformations of the detailed micro-model for comparison. More precisely, we perform three regressions for each sample. The key idea is to minimize the squared error of the total elastic stored energy and of the two control angles ψ at probe points, evaluated with the previously mentioned models. The probe points are the center of the specimen C and the corner of the 'quasi-rigid' triangle near a base of the specimen V (see Fig. 2). These two angles are chosen because each of them is mainly related to one of the energy terms of the macro-model. Indeed, the energy involved in the distortion angle at the center is mostly governed by the parameter K_p, while the distortion angle at the triangle vertex depends for the

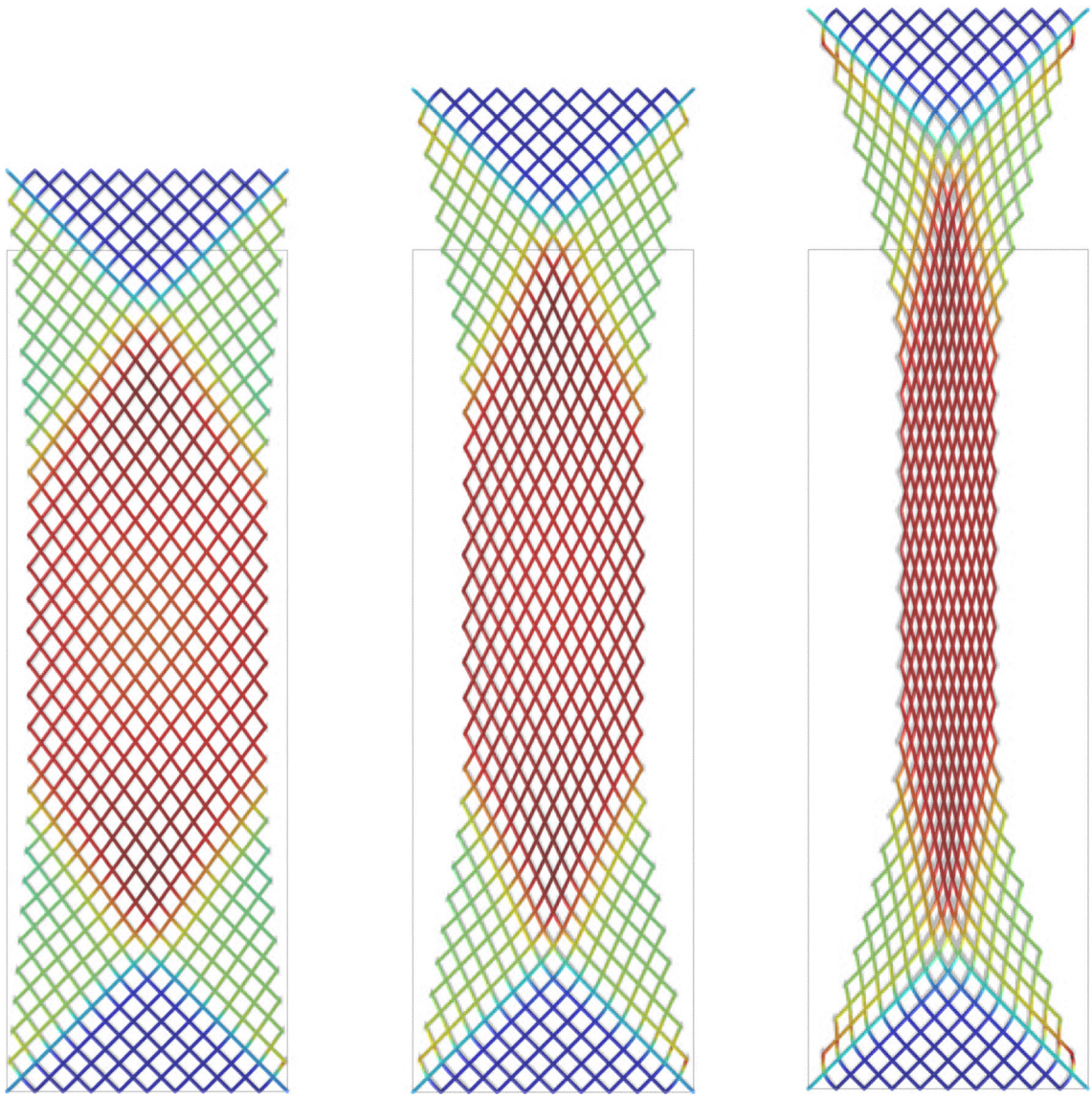

FIG. 5. Overlap between simulation with micro-Cauchy model (*gray*) and with macro-second gradient model (*colors*, which indicate the shear distortion γ) for the sample n. 1. Bias extension test with imposed displacement $u_0 = \{2, 4, 6\}$ cm (color figure online)

most part on the bending energy characterized by K_{II}. Finally, the last parameter K_{I} can be derived by considering the whole stored energy.

Table 3 shows the fitting results obtained through a numerical investigation conducted by the FEM environment COMSOL Multiphysics for the considered samples. Specifically, we use a standard finite element formulation for the micro-model, while a Hellinger–Reissner variational principle is employed to adapt standard FE tools developed for first gradient continuum to a second gradient continuum as the one considered for the macro-model. In detail, we introduce two auxiliary fields $\boldsymbol{M}$ and $\boldsymbol{\Lambda}$ and recast only second gradient terms of the energy density (2.13), i.e.,

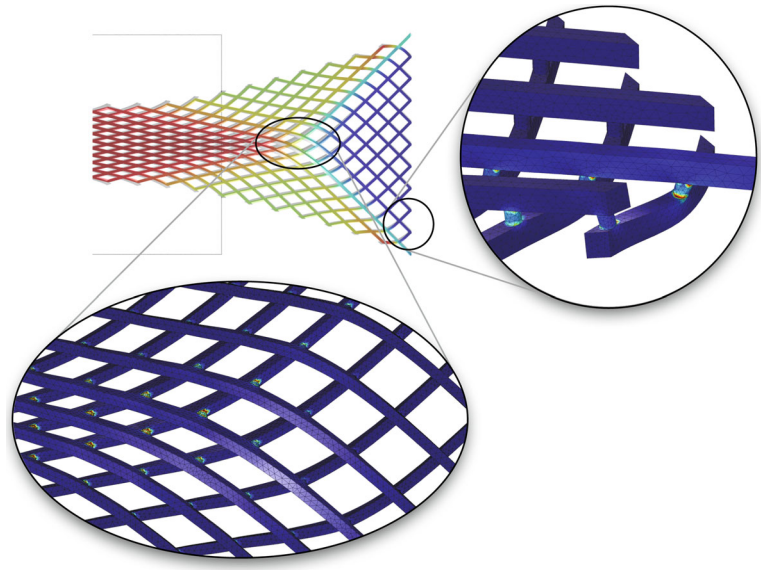

FIG. 6. 3D deformation details for the sample n. 1; the *colors* in the *zooms* indicate the stored elastic energy density (color figure online)

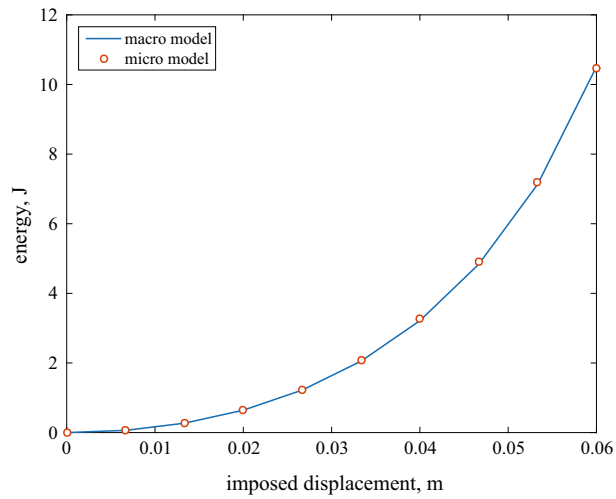

FIG. 7. Sample n. 2: Comparison of the total energy between the micro-Cauchy model (*points*) and a macro-second gradient model (*solid line*)

$$W_M^{(\kappa_\alpha)}(\nabla \boldsymbol{u}, \nabla\nabla \boldsymbol{u}) = \frac{1}{2} K_{\mathrm{II}} \kappa_\alpha^2 (\nabla \boldsymbol{u}, \nabla\nabla \boldsymbol{u}) \tag{3.1}$$

considering the extended energy density, which involves only first gradient contributions, as follows

$$\hat{W}_M^{(\kappa_\alpha)}(\nabla \boldsymbol{u}, \boldsymbol{M}, \nabla \boldsymbol{M}) = \frac{1}{2} K_{\mathrm{II}} \hat{\kappa}_\alpha^2 (\boldsymbol{M}, \nabla \boldsymbol{M}) + \boldsymbol{\Lambda}\,(\boldsymbol{M} - \nabla \boldsymbol{u}) \tag{3.2}$$

where $\boldsymbol{\Lambda}$ could be interpreted as a field of Lagrange multipliers.

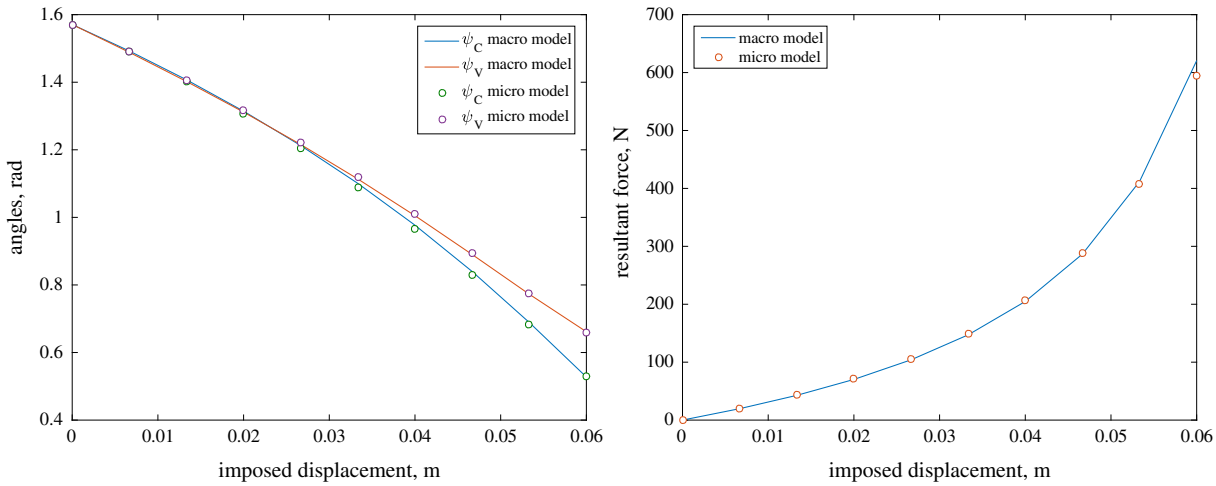

FIG. 8. Sample n. 2: Comparisons between the micro-Cauchy model (*points*) and a macro-second gradient model (*solid line*). Angle at center (*blue line*), angle at corner (*red line*) on the *left*; total reaction on the *right* (color figure online)

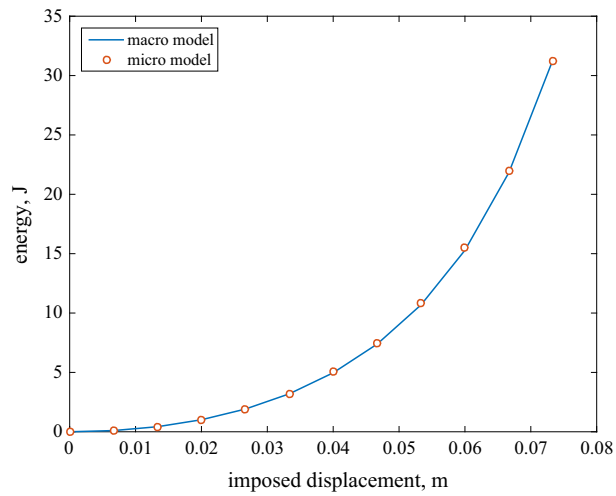

FIG. 9. Sample n. 3: Comparison of the total energy between the micro-Cauchy model (*points*) and a macro-second gradient model (*solid line*)

The results of Table 3 clearly show the presence of a coupling between the different energy contributions of the macro-model. Indeed, by changing the aspect ratio h_p/d_p of the pivot, a change in the extensional and flexural rigidity of the fibers is also observed notwithstanding they retain the same cross section.

In Figs. 3 and 4(left), the total energy and the angles ψ_C and ψ_V used for fitting the macro-model are shown as the imposed displacement relative to the bias test is varying. In Fig. 4(right), in order to get a better insight into the regression results, a comparison between the total reaction of the micro-model and the one evaluated with the macro-model is plotted versus the imposed displacement. As far as relatively small displacement are concerned, the accordance between the two models is quite satisfactory while at $u_0 = 6$ cm a discrepancy is observed (see also Fig. 5). This phenomenon can be explained by

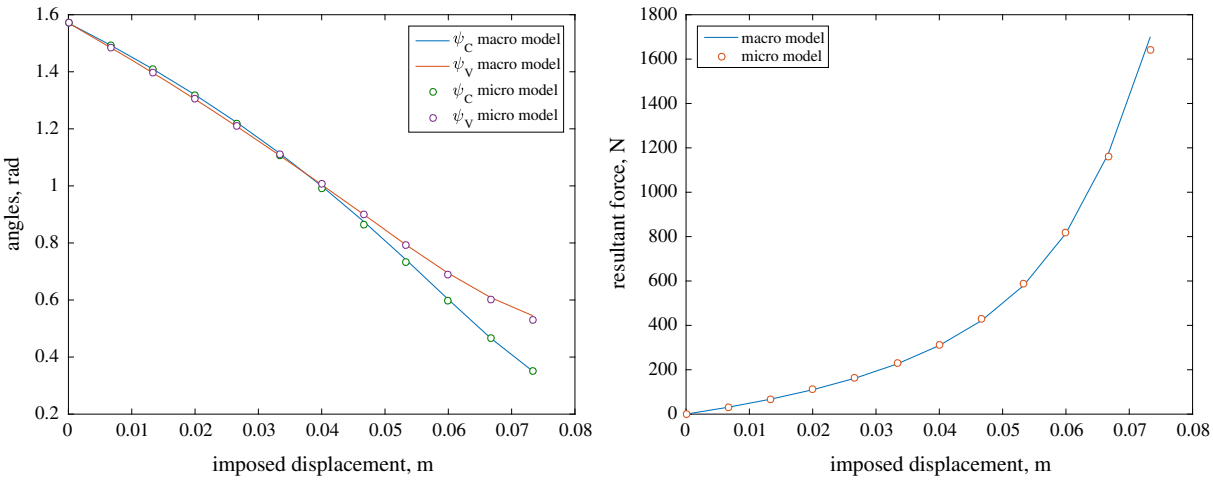

FIG. 10. Sample n. 3: Comparisons between the micro-Cauchy model (*points*) and a macro-second gradient model (*solid line*). Angle at center (*blue line*), angle at corner (*red line*) on the *left*; total reaction on the *right* (color figure online)

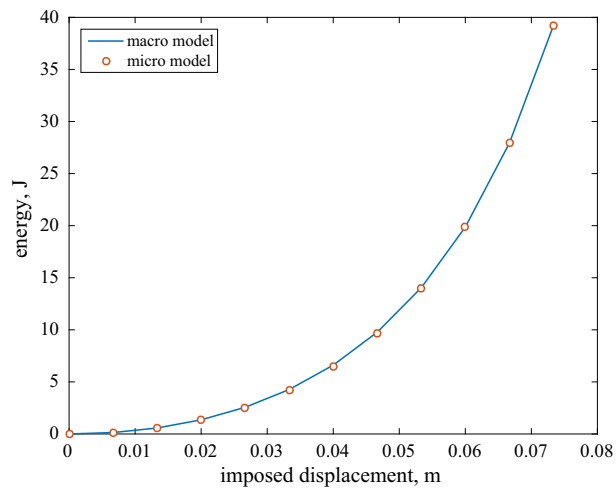

FIG. 11. Sample n. 4: Comparison of the total energy between the micro-Cauchy model (*points*) and a macro-second gradient model (*solid line*) (color figure online)

considering that the micro-model has a richer kinematics than the macro one. Indeed, the former model allows twist and possibly out-of-plane bending of fibers to occur as well as shear distortion, bending and possibly extension of pivots, while the latter model does not. We observe (see Fig. 6) that for the more refined micro-model a non-negligible amount of energy is stored as deformation energy for configurations which are not accounted for in the coarser macro-model. Therefore, equating the two total energies of the examined models and evaluating the constraint reactions—which can be computed as the first derivatives of the energies with respect to the imposed displacement—we expect a discrepancy between the two reactions. Looking at Fig. 4(right), we can confirm this last statement at the largest displacement, which is likely to be the one where deformation energies due to the richer kinematics of the refined model start to acquire significance.

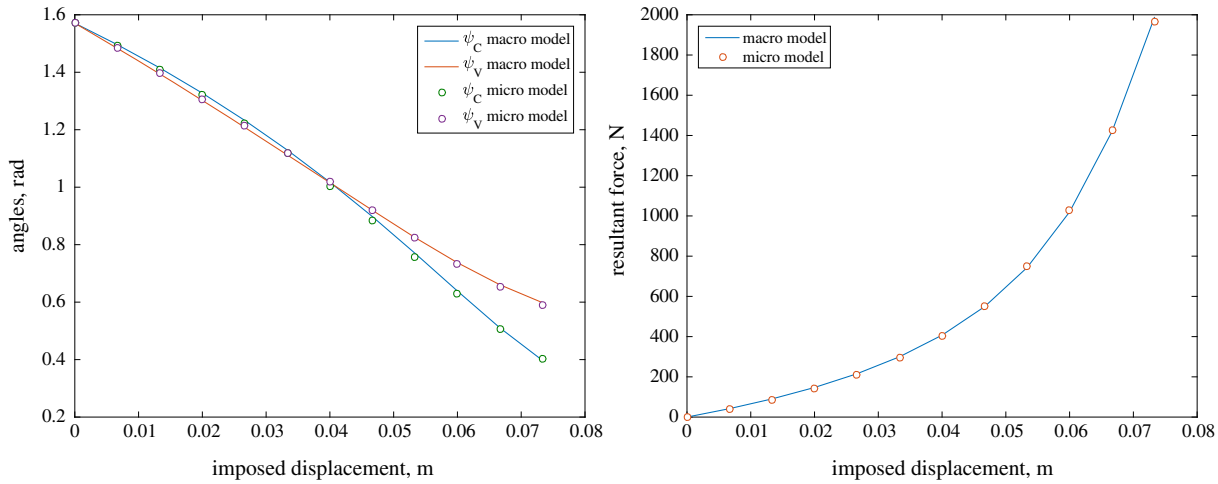

FIG. 12. Sample n. 4: Comparisons between the micro-Cauchy model (*points*) and a macro-second gradient model (*solid line*). Angle at center (*blue line*), angle at corner (*red line*) on the *left*; total reaction on the *right* (color figure online)

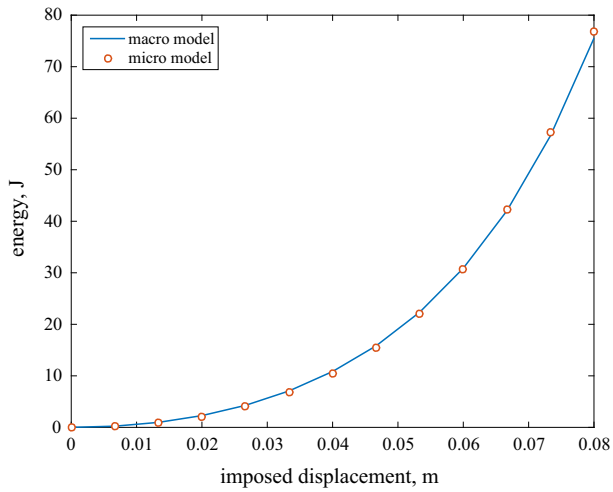

FIG. 13. Sample n. 5: Comparison of the total energy between the micro-Cauchy model (*points*) and a macro-second gradient model (*solid line*)

For all the samples under study, we perform the same identification procedure and the results are shown in Figs. 7, 8, 9, 10, 11, 12, 13, 14, 15 and 16. Similar considerations can be made for all samples as those already made for the first one. Moreover, we note that different slenderness of the pivots results in a different discrepancy of the reaction force between the two models at the largest displacement. Indeed, for samples n. 1, 2 and 3, the macro-model exhibits a greater reaction force than the micro-model, while the opposite occurs for samples n. 5 and 6. This effect may be due to the fact that the energy associated with the richer micro kinematics could contribute to the overall reaction, and therefore, we might either overestimate or underestimate this reaction; sometimes also a compensation of this effect might happen as in the case of sample n. 4.

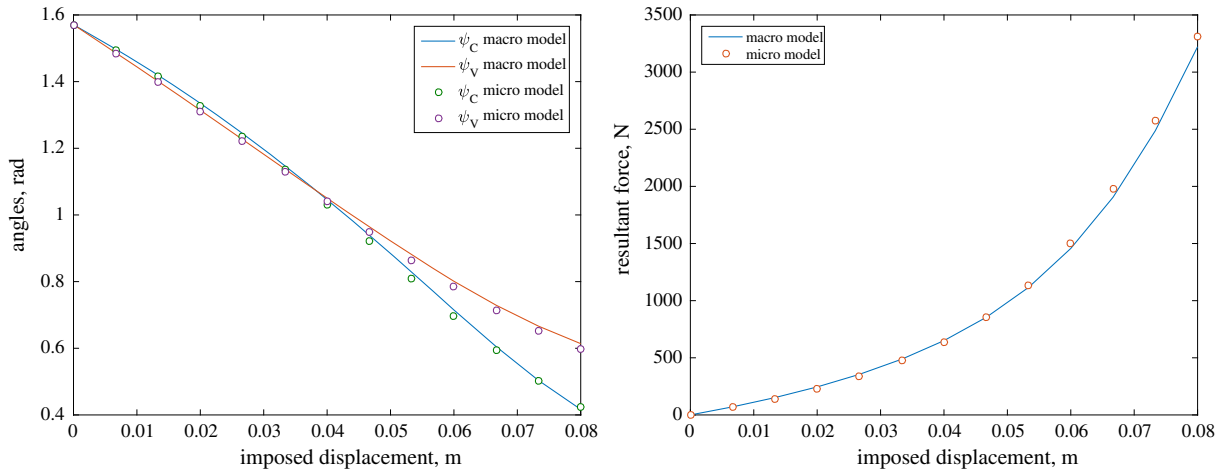

FIG. 14. Sample n. 5: Comparisons between the micro-Cauchy model (*points*) and a macro-second gradient model (*solid line*). Angle at center (*blue line*), angle at corner (*red line*) on the *left*; total reaction on the *right* (color figure online)

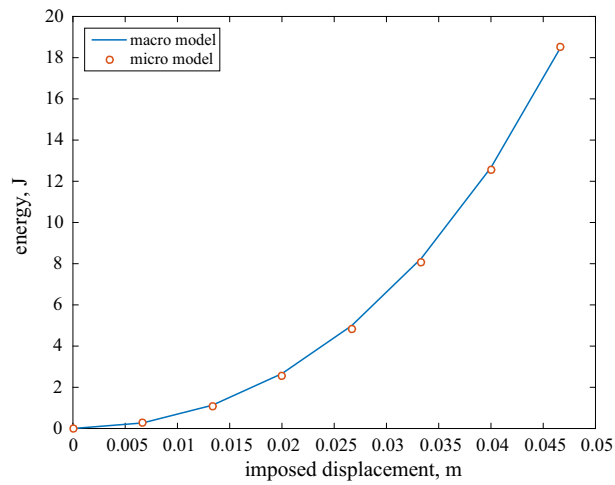

FIG. 15. Sample n. 6: Comparison of the total energy between the micro-Cauchy model (*points*) and a macro-second gradient model (*solid line*)

In order to test the degree of predictivity of the macro-model proposed, we also compare the two models in a different test in which a relative rotation and elongation of short sides are imposed (see, for instance, the test carried out on the sample n. 5 in Fig. 17). We see a good agreement between the models, as remarked above, if the three-dimensional equilibrium shape remains in plane without twist and out-of-plane bending of fibers as well as shear distortion, bending and extension of pivots.

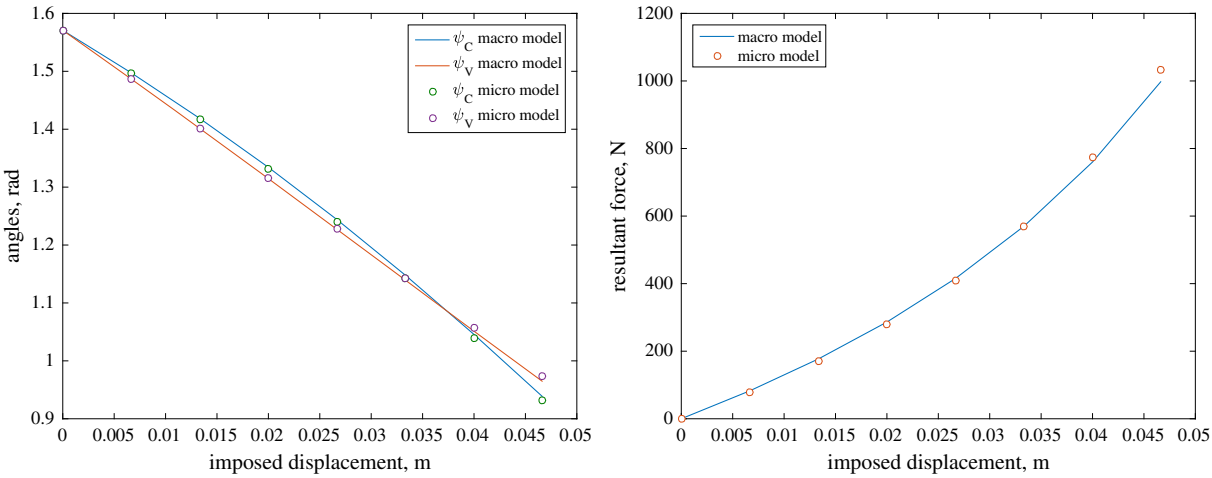

FIG. 16. Sample n. 6: Comparisons between the micro-Cauchy model (*points*) and a macro-second gradient model (*solid line*). Angle at center (*blue line*), angle at corner (*red line*) on the *left*; total reaction on the *right* (color figure online)

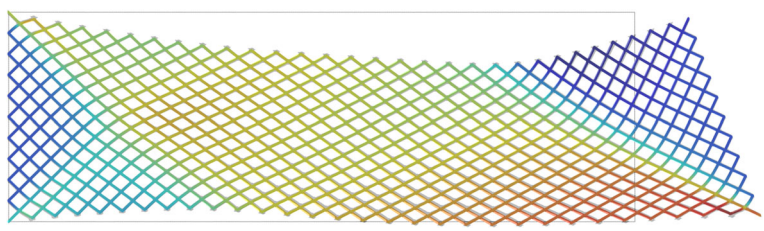

FIG. 17. Overlap between simulation with micro-Cauchy model (*gray*) and with macro-second gradient model (*colors*, which indicate the shear distortion γ) for the sample n. 5. Generalized bias test with imposed displacement $u_0 = 3$ cm and rotation $\theta = 20$ degrees (color figure online)

4. Conclusions

In this paper, we consider two models aimed at describing the behavior of pantographic structures. At a relatively small length scale, a micro-model based on Cauchy first gradient continuum theories is adopted in order to provide an accurate description of the geometry, and the deformation of the elastic pivots which represent a crucial point in modeling these structures. This choice unluckily requires a heavy computational load with the finite element method because a high number of degrees of freedom is involved, even if one considers a small specimen as done experimentally in [34].

On the other hand, we consider a higher gradient reduced-order model characterized by a length scale in which the elastic pivots have negligible dimensions. Such a macro-model has predictive performances absolutely compatible with the more refined micro-model but a lower computational cost. For this macro-model, the significant amount of elastic energy stored in the pivots is taken into account by means of a suitable elastic potential related to the shear distortion, i.e., the change in the angle between the fibers 'intersecting' at the same pivot.

Herein, we compare the two models and perform a numerical identification of the material parameters characterizing the macro-model having assumed fixed and known those of the micro-model, considered as a reference model.

We, finally, observe that when the more detailed micro-model exhibits a significant three-dimensional deformation, the agreement between the two models is lost. Of course, this is an expected result because the macro-model is characterized by planar motion and therefore is not able to describe such a 3D deformation.

References

1. Alibert, J.-J., Della Corte, A.: Second-gradient continua as homogenized limit of pantographic microstructured plates: a rigorous proof. Z. Angew. Math. Phys. **66**(5), 2855–2870 (2015)
2. Alibert, J.-J., Seppecher, P., Dell'Isola, F.: Truss modular beams with deformation energy depending on higher displacement gradients. Math. Mech. Solids **8**(1), 51–73 (2003)
3. Altenbach, H., Eremeyev, V.A.: On the linear theory of micropolar plates. ZAMM-Z. Angew. Math. Mech. **89**(4), 242–256 (2009)
4. Aminpour, H., Rizzi, N.: On the modelling of carbon nano tubes as generalized continua. In: Altenbach, H., Forest, S. (eds.) Generalized Continua as Models for Classical and Advanced Materials, vol. 42, pp. 15–35. Springer, Switzerland (2016)
5. AminPour, H., Rizzi, N.: A one-dimensional continuum with microstructure for single-wall carbon nanotubes bifurcation analysis. Math. Mech. Solids **21**(2), 168–181 (2016)
6. Aminpour, H., Rizzi, N., Salerno, G.: A one-dimensional beam model for single-wall carbon nano tube column buckling. In: Civil-comp Proceedings (2014)
7. Andreaus, U., Baragatti, P., Placidi, L.: Experimental and numerical investigations of the responses of a cantilever beam possibly contacting a deformable and dissipative obstacle under harmonic excitation. Int. J. Non-Linear Mech. **80**, 96–106 (2016)
8. Andreaus, U., Baragatti, P., Placidi, L.: Soft-impact dynamics of deformable bodies. Contin. Mech. Thermodyn. **25**(3), 375–398 (2013)
9. Caggegi, C., Pensée, V., Fagone, M., Cuomo, M., Chevalier, L.: Experimental global analysis of the efficiency of carbon fiber anchors applied over CFRP strengthened bricks. Constr. Build. Mater. **53**, 203–212 (2014)
10. Carassale, L., Piccardo, G.: Non-linear discrete models for the stochastic analysis of cables in turbulent wind. Int. J. Non-Linear Mech. **45**(3), 219–231 (2010)
11. Carcaterra, A., Akay, A., Bernardini, C.: Trapping of vibration energy into a set of resonators: theory and application to aerospace structures. Mech. Syst. Signal Process. **26**, 1–14 (2012)
12. Carcaterra, A., D'Ambrogio, W.: An iterative rational fraction polynomial technique for modal identification. Meccanica **30**(1), 63–75 (1995)
13. Carcaterra, A., Dell'Isola, F., Esposito, R., Pulvirenti, M.: Macroscopic description of microscopically strongly inhomogenous systems: a mathematical basis for the synthesis of higher gradients metamaterials. Arch. Ration. Mech. Anal. **218**, 1239–1262 (2015)
14. Carcaterra, A., Roveri, N.: Tire grip identification based on strain information: theory and simulations. Mech. Syst. Signal Process. **41**(1), 564–580 (2013)
15. Cazzani, A., Garusi, E., Tralli, A., Atluri, S.N.: A four-node hybrid assumed-strain finite element for laminated composite plates. CMC: Comput. Mater. Contin. **2**(1), 23–38 (2005)
16. Cazzani, A., Lovadina, C.: On some mixed finite element methods for plane membrane problems. Comput. Mech. **20**(6), 560–572 (1997)
17. Cazzani, A., Malagù, M., Turco, E.: Isogeometric analysis of plane-curved beams. Math. Mech. Solids (2014). doi:10.1177/1081286514531265
18. Cazzani, A., Malagù, M., Turco, E., Stochino, F.: Constitutive models for strongly curved beams in the frame of isogeometric analysis. Math. Mech. Solids **21**(2), 182–209 (2016)
19. Cazzani, A., Stochino, F., Turco, E.: An analytical assessment of finite element and isogeometric analyses of the whole spectrum of Timoshenko beams. ZAMM-Z. Angew. Math. Mech. (2016). doi:10.1002/zamm.201500280
20. Challamel, N., Lerbet, J., Wang, C.M., Zhang, Z.: Analytical length scale calibration of nonlocal continuum from a microstructured buckling model. ZAMM-Z. Angew. Math. Mech. **94**(5), 402–413 (2014)
21. Challamel, N., Zhang, Z., Wang, C.M.: Nonlocal equivalent continua for buckling and vibration analyses of microstructured beams. J. Nanomech. Micromech. **5**, A4014004 (2014)
22. Cuomo, M., Dell'Isola, F., Greco, L.: Simplified analysis of a generalized bias-test for fabrics with two families of inextensible fibres. ZAMP-Z. Angew. Math. Phys. (2016). doi:10.1007/s00033-016-0653-z
23. D'Agostino, M.V., Giorgio, I., Greco, L., Madeo, A., Boisse, P.: Continuum and discrete models for structures including (quasi-) inextensible elasticae with a view to the design and modeling of composite reinforcements. Int. J. Solids Struct. **59**, 1–17 (2015)

24. D'Annibale, F., Luongo, A.: A damage constitutive model for sliding friction coupled to wear. Contin. Mech. Thermodyn. **25**(2–4), 503–522 (2013)
25. D'Annibale, F., Rosi, G., Luongo, A.: Linear stability of piezoelectric-controlled discrete mechanical systems under nonconservative positional forces. Meccanica **50**(3), 825–839 (2015)
26. D'Annibale, F., Rosi, G., Luongo, A.: On the failure of the 'similar piezoelectric control' in preventing loss of stability by nonconservative positional forces. Z. Angew. Math. Phys. **66**(4), 1949–1968 (2015)
27. Del Vescovo, D., Fregolent, A.: Theoretical and experimental dynamic analysis aimed at the improvement of an acoustic method for fresco detachment diagnosis. Mech. Syst. Signal Process. **23**(7), 2312–2319 (2009)
28. Del Vescovo, D., Giorgio, I.: Dynamic problems for metamaterials: review of existing models and ideas for further research. Int. J. Eng. Sci. **80**, 153–172 (2014)
29. Della Corte, A., Battista, A., Dell'Isola, F.: Referential description of the evolution of a 2D swarm of robots interacting with the closer neighbors: perspectives of continuum modeling via higher gradient continua. Int. J. Non-Linear Mech. **80**, 209–220 (2016)
30. Dell'Isola, F., Andreaus, U., Placidi, L.: At the origins and in the vanguard of peridynamics, non-local and higher-gradient continuum mechanics: an underestimated and still topical contribution of Gabrio Piola. Math. Mech. Solids **20**(8), 887–928 (2015)
31. Dell'Isola, F., D'Agostino, M.V., Madeo, A., Boisse, P., Steigmann, D.J.: Minimization of shear energy in two dimensional continua with two orthogonal families of inextensible fibers: the case of standard bias extension test. J. Elast. **122**(2), 131–155 (2016)
32. Dell'Isola, F., Della Corte, A., Greco, L., Luongo, A.: Plane bias extension test for a continuum with two inextensible families of fibers: a variational treatment with Lagrange multipliers and a perturbation solution. Int. J. Solids Struct. **81**, 1–12 (2016)
33. Dell'Isola, F., Giorgio, I., Pawlikowski, M., Rizzi, N.L.: Large deformations of planar extensible beams and pantographic lattices: heuristic homogenization, experimental and numerical examples of equilibrium. Proc. R. Soc. Lond. A **472**(2185), 20150790 (2016)
34. Dell'Isola, F., Lekszycki, T., Pawlikowski, M., Grygoruk, R., Greco, L.: Designing a light fabric metamaterial being highly macroscopically tough under directional extension: first experimental evidence. Z. Angew. Math. Phys. **66**(6), 3473–3498 (2015)
35. Dell'Isola, F., Madeo, A., Seppecher, P.: Cauchy tetrahedron argument applied to higher contact interactions. Arch. Ration. Mech. Anal. **219**(3), 1305–1341 (2016)
36. Dell'Isola, F., Maier, G., Perego, U., Andreaus, U., Esposito, R., Forest, S.: The complete works of Gabrio Piola: volume I—commented english translation. Adv. Struct. Mater. (2014). doi:10.1007/978-3-319-00263-7
37. Dell'Isola, F., Seppecher, P., Della Corte, A.: The postulations á la D'Alembert and á la Cauchy for higher gradient continuum theories are equivalent: a review of existing results. Proc. R. Soc. Lond. A **471**(2183), 20150415 (2015)
38. Dell'Isola, F., Seppecher, P., Madeo, A.: How contact interactions may depend on the shape of Cauchy cuts in Nth gradient continua: approach "à la D'Alembert". Z. Angew. Math. Phys. **63**(6), 1119–1141 (2012)
39. Dell'Isola, F., Steigmann, D.: A two-dimensional gradient-elasticity theory for woven fabrics. J. Elast. **118**(1), 113–125 (2015)
40. Dell'Isola, F., Steigmann, D., Della Corte, A.: Synthesis of fibrous complex structures: designing microstructure to deliver targeted macroscale response. Appl. Mech. Rev. **67**(6), 060804 (2015)
41. Dietrich, L., Lekszycki, T., Turski, K.: Problems of identification of mechanical characteristics of viscoelastic composites. Acta Mech. **126**(1–4), 153–167 (1998)
42. Dos Reis, F., Ganghoffer, J.F.: Construction of micropolar continua from the asymptotic homogenization of beam lattices. Comput. Struct. **112**, 354–363 (2012)
43. Eremeyev, V.A., Pietraszkiewicz, W.: Material symmetry group and constitutive equations of micropolar anisotropic elastic solids. Math. Mech. Solids **21**(2), 210–221 (2016)
44. Eringen, A.C.: Mechanics of Micromorphic Continua. Springer, New York (1968)
45. Eringen, A.C.: Nonlocal Continuum Field Theories. Springer, New York (2002)
46. Evdokymov, N., Altenbach, H., Eremeyev, V.A.: Collapse criteria of foam cells under various loading. PAMM **11**(1), 365–366 (2011)
47. Federico, S., Gasser, T.C.: Nonlinear elasticity of biological tissues with statistical fibre orientation. J. R. Soc. Interface **7**(47), 955–966 (2010)
48. Federico, S., Grillo, A.: Elasticity and permeability of porous fibre-reinforced materials under large deformations. Mech. Mater. **44**, 58–71 (2012)
49. Frischmuth, K., Kosiński, W., Lekszycki, T.: Free vibrations of finite-memory material beams. Int. J. Eng. Sci. **31**(3), 385–395 (1993)
50. Gabriele, S., Rizzi, N., Varano, V.: On the imperfection sensitivity of thin-walled frames. In: Civil-Comp Proceedings, p. 99 (2012)

51. Gabriele, S., Rizzi, N., Varano, V.: A one-dimensional nonlinear thin walled beam model derived from Koiter shell theory. In: Civil-Comp Proceedings, p. 106 (2014)
52. Gabriele, S., Rizzi, N., Varano, V.: A 1D nonlinear TWB model accounting for in plane cross-section deformation. Int. J. Solids Struct. (2016). doi:10.1016/j.ijsolstr.2016.04.017
53. Giorgio, I., Grygoruk, R., Dell'Isola, F., Steigmann, D.J.: Pattern formation in the three-dimensional deformations of fibered sheets. Mech. Res. Commun. **69**, 164–171 (2015)
54. Goda, I., Assidi, M., Ganghoffer, J.-F.: Equivalent mechanical properties of textile monolayers from discrete asymptotic homogenization. J. Mech. Phys. Solids **61**(12), 2537–2565 (2013)
55. Goda, I., Assidi, M., Ganghoffer, J.F.: A 3D elastic micropolar model of vertebral trabecular bone from lattice homogenization of the bone microstructure. Biomech. Model. Mechanobiol. **13**(1), 53–83 (2014)
56. Greco, L., Cuomo, M.: On the force density method for slack cable nets. Int. J. Solids Struct. **49**(13), 1526–1540 (2012)
57. Greco, L., Cuomo, M.: An implicit G1 multi patch B-spline interpolation for Kirchhoff-Love space rod. Comput. Methods Appl. Mech. Eng. **269**, 173–197 (2014)
58. Greco, L., Cuomo, M.: Consistent tangent operator for an exact Kirchhoff rod model. Contin. Mech. Thermodyn. **27**(4), 861–877 (2015)
59. Greco, L., Cuomo, M.: An isogeometric implicit G1 mixed finite element for Kirchhoff space rods. Comput. Methods Appl. Mech. Eng. **298**, 325–349 (2016)
60. Greco, L., Impollonia, N., Cuomo, M.: A procedure for the static analysis of cable structures following elastic catenary theory. Int. J. Solids Struct. **51**(7), 1521–1533 (2014)
61. Green, A.E., Rivlin, R.S.: Multipolar continuum mechanics. Arch. Ration. Mech. Anal. **17**(2), 113–147 (1964)
62. Grillo, A., Federico, S., Wittum, G.: Growth, mass transfer, and remodeling in fiber-reinforced, multi-constituent materials. Int. J. Non-Linear Mech. **47**(2), 388–401 (2012)
63. Grillo, A., Wittum, G., Tomic, A., Federico, S.: Remodelling in statistically oriented fibre-reinforced materials and biological tissues. Math. Mech. Solids **20**(9), 1107–1129 (2015)
64. Hans, S., Boutin, C.: Dynamics of discrete framed structures: a unified homogenized description. J. Mech. Mater. Struct. **3**(9), 1709–1739 (2008)
65. Harrison, P.: Modelling the forming mechanics of engineering fabrics using a mutually constrained pantographic beam and membrane mesh. Compos. Part A Appl. Sci. Manuf. **81**, 145–157 (2016)
66. Harrison, P., Abdiwi, F., Guo, Z., Potluri, P., Yu, W.R.: Characterising the shear-tension coupling and wrinkling behaviour of woven engineering fabrics. Compos. Part A Appl. Sci. Manuf. **43**(6), 903–914 (2012)
67. Harrison, P., Clifford, M.J., Long, A.C.: Shear characterisation of viscous woven textile composites: a comparison between picture frame and bias extension experiments. Compos. Sci. Technol. **64**(10), 1453–1465 (2004)
68. Härtel, F., Harrison, P.: Evaluation of normalisation methods for uniaxial bias extension tests on engineering fabrics. Compos. Part A Appl. Sci. Manuf. **67**, 61–69 (2014)
69. Lekszycki, T., Dell'Isola, F.: A mixture model with evolving mass densities for describing synthesis and resorption phenomena in bones reconstructed with bio-resorbable materials. Z. Angew. Math. Mech. **92**(6), 426–444 (2012)
70. Lekszycki, T., Olhoff, N., Pedersen, J.J.: Modelling and identification of viscoelastic properties of vibrating sandwich beams. Compos. Struct. **22**(1), 15–31 (1992)
71. Luongo, A., Zulli, D., Piccardo, G.: On the effect of twist angle on nonlinear galloping of suspended cables. Comput. Struct. **87**(15), 1003–1014 (2009)
72. Mindlin, R.D.: Micro-structure in linear elasticity. Arch. Ration. Mech. Anal. **16**(1), 51–78 (1964)
73. Mindlin, R.D.: Second gradient of strain and surface-tension in linear elasticity. Int. J. Solids Struct. **1**(4), 417–438 (1965)
74. Nadler, B., Steigmann, D.J.: A model for frictional slip in woven fabrics. C. R. Mec. **331**(12), 797–804 (2003)
75. Nikopour, H., Selvadurai, A.P.S.: Torsion of a layered composite strip. Compos. Struct. **95**, 1–4 (2013)
76. Nikopour, H., Selvadurai, A.P.S.: Concentrated loading of a fibre-reinforced composite plate: experimental and computational modeling of boundary fixity. Compos. Part B Eng. **60**, 297–305 (2014)
77. Pideri, C., Seppecher, P.: A second gradient material resulting from the homogenization of an heterogeneous linear elastic medium. Contin. Mech. Thermodyn. **9**(5), 241–257 (1997)
78. Pignataro, M., Ruta, G., Rizzi, N., Varano, V.: Effects of warping constraints and lateral restraint on the buckling of thin-walled frames. In: ASME 2009 International Mechanical Engineering Congress and Exposition, pp. 803–810. American Society of Mechanical Engineers, 2009
79. Placidi, L.: A variational approach for a nonlinear 1-dimensional second gradient continuum damage model. Contin. Mech. Thermodyn. **27**(4), 623–638 (2015)
80. Placidi, L.: A variational approach for a nonlinear one-dimensional damage-elasto-plastic second-gradient continuum model. Contin. Mech. Thermodyn. **28**(1), 119–137 (2016)
81. Placidi, L., Andreaus, U., Della Corte, A., Lekszycki, T.: Gedanken experiments for the determination of two-dimensional linear second gradient elasticity coefficients. Z. Angew. Math. Phys. **66**(6), 3699–3725 (2015)
82. Placidi, L., Andreaus, U., Giorgio, I.: Identification of two-dimensional pantographic structure via a linear D4 orthotropic second gradient elastic model. J. Eng. Math. (2016). doi:10.1007/s10665-016-9856-8

83. Rinaldi, A., Placidi, L.: A microscale second gradient approximation of the damage parameter of quasi-brittle heterogeneous lattices. ZAMM-Z. Angew. Math. Mech. **94**(10), 862–877 (2014)
84. Rizzi, N., Varano, V.: On the postbuckling analysis of thin-walled frames. In: Thirteenth International Conference on Civil, Structural and Environmental Engineering Computing. Civil-Comp Press (2011)
85. Rizzi, N.L., Varano, V.: The effects of warping on the postbuckling behaviour of thin-walled structures. Thin-Walled Struct. **49**(9), 1091–1097 (2011)
86. Rizzi, N.L., Varano, V., Gabriele, S.: Initial postbuckling behavior of thin-walled frames under mode interaction. Thin-Walled Struct. **68**, 124–134 (2013)
87. Roveri, N., Carcaterra, A.: Damage detection in structures under traveling loads by Hilbert–Huang transform. Mech. Syst. Signal Process. **28**, 128–144 (2012)
88. Ruta, G.C., Varano, V., Pignataro, M., Rizzi, N.L.: A beam model for the flexural–torsional buckling of thin-walled members with some applications. Thin-Walled Struct. **46**(7–9), 816–822 (2008)
89. Scerrato, D., Giorgio, I., Rizzi, N.L.: Three-dimensional instabilities of pantographic sheets with parabolic lattices: numerical investigations. Z. Angew. Math. Phys.-ZAMP. (2016). doi:10.1007/s00033-016-0650-2
90. Scerrato, D., Zurba Eremeeva, I.A., Lekszycki, T., Rizzi, N.L.: On the effect of shear stiffness on the plane deformation of linear second gradient pantographic sheets. Z. Angew. Math. Mech.-ZAMM. (2016). doi:10.1002/zamm201600066
91. Selvadurai, A.P.S., Nikopour, H.: Transverse elasticity of a unidirectionally reinforced composite with an irregular fibre arrangement: experiments, theory and computations. Compos. Struct. **94**(6), 1973–1981 (2012)
92. Seppecher, P., Alibert, J.-J., Dell'Isola, F.: Linear elastic trusses leading to continua with exotic mechanical interactions. J. Phys. Conf. Ser. **319**(1), 012018 (2011)
93. Solari, G., Pagnini, L.C., Piccardo, G.: A numerical algorithm for the aerodynamic identification of structures. J. Wind Eng. Ind. Aerodyn. **69**, 719–730 (1997)
94. Steigmann, D.J.: Theory of elastic solids reinforced with fibers resistant to extension, flexure and twist. Int. J. Non-Linear Mech. **47**(7), 734–742 (2012)
95. Steigmann, D.J., Dell'Isola, F.: Mechanical response of fabric sheets to three-dimensional bending, twisting, and stretching. Acta Mech. Sin. **31**(3), 373–382 (2015)
96. Steigmann, D.J., Pipkin, A.C.: Equilibrium of elastic nets. Philos. Trans. R. Soc. Lond. A Math. Phys. Eng. Sci. **335**(1639), 419–454 (1991)
97. Tomic, A., Grillo, A., Federico, S.: Poroelastic materials reinforced by statistically oriented fibres - numerical implementation and application to articular cartilage. IMA J. Appl. Math. **79**, 1027–1059 (2014)
98. Toupin, R.A.: Theories of elasticity with couple-stress. Arch. Ration. Mech. Anal. **17**(2), 85–112 (1964)
99. Turco, E.: Is the statistical approach suitable for identifying actions on structures. Comput. Struct. **83**(25), 2112–2120 (2005)
100. Turco, E., Aristodemo, M.: A three-dimensional B-spline boundary element. Comput. Methods Appl. Mech. Eng. **155**(1), 119–128 (1998)
101. Turco, E., Caracciolo, P.: Elasto-plastic analysis of Kirchhoff plates by high simplicity finite elements. Comput. Methods Appl. Mech. Eng. **190**(5), 691–706 (2000)
102. Turco, E., Dell'Isola, F., Cazzani, A., Rizzi, N.L.: Hencky-type discrete model for pantographic structures: numerical comparison with second gradient continuum models. Z. Angew. Math. Phys. (2016). doi:10.1007/s00033-016-0681-8
103. Yang, Y., Ching, W.Y., Misra, A.: Higher-order continuum theory applied to fracture simulation of nanoscale intergranular glassy film. J. Nanomech. Micromechan. **1**(2), 60–71 (2011)
104. Yang, Y., Misra, A.: Higher-order stress-strain theory for damage modeling implemented in an element-free Galerkin formulation. Comput. Model. Eng. Sci. (CMES) **64**(1), 1–36 (2010)

Ivan Giorgio
Department of Structural and Geotechnical Engineering
Università di Roma La Sapienza
Rome, Italy
e-mail: ivan.giorgio@uniroma1.it

Ivan Giorgio
International Research Center for the Mathematics and Mechanics of Complex Systems - MeMoCS
Università dell'Aquila
Cisterna di Latina, Italy

(Received: April 27, 2016)